Monthly Notices
of the
ROYAL ASTRONOMICAL SOCIETY

MNRAS **465,** 4690–4702 (2017)
Advance Access publication 2016 November 22

doi:10.1093/mnras/stw2998

K-shell photoionization of O^{4+} and O^{5+} ions: experiment and theory

B. M. McLaughlin,[1,2★] J.-M. Bizau,[3,4★] D. Cubaynes,[3,4] S. Guilbaud,[3] S. Douix,[4] M. M. Al Shorman,[5] M. O. A. El Ghazaly,[6] I. Sakho[7] and M. F. Gharaibeh[8★†]

[1]*Centre for Theoretical Atomic and Molecular Physics (CTAMOP), School of Mathematics and Physics, Queen's University Belfast, Belfast BT7 1NN, UK*
[2]*Institute for Theoretical Atomic and Molecular Physics (ITAMP), Harvard–Smithsonian Center for Astrophysics, MS-14, Cambridge, MA 02138, USA*
[3]*Institut des Sciences Moléculaires d'Orsay (ISMO), CNRS UMR 8214, Université Paris-Sud, Université Paris-Saclay, F-91405 Orsay cedex, France*
[4]*Synchrotron SOLEIL – L'Orme des Merisiers, Saint-Aubin – BP 48, F-91192 Gif-sur-Yvette cedex, France*
[5]*Applied Physics Department, Faculty of Science, Tafila Technical University, Tafila 66110, Jordan*
[6]*Astrophysics and Space Sciences Section, Jet Propulsion Laboratory, Caltech, Pasadena, CA 91109, USA*
[7]*Department of Physics, UFR of Sciences and Technologies, University Assane Seck of Ziguinchor, Ziguinchor, Senegal*
[8]*Department of Mathematics, Statistics and Physics, PO Box 2713, Qatar University, Doha, Qatar*

Accepted 2016 November 16. Received 2016 November 13; in original form 2016 September 7

ABSTRACT

Absolute cross-sections for the *K*-shell photoionization of Be-like (O^{4+}) and Li-like (O^{5+}) atomic oxygen ions were measured for the first time (in their respective *K*-shell regions) by employing the ion–photon merged-beam technique at the SOLEIL synchrotron-radiation facility in Saint-Aubin, France. High-resolution spectroscopy with $E/\Delta E \approx 3200$ ($\approx$170 meV, full width at half-maximum) was achieved with photon energy from 550 to 670 eV. Rich resonance structure observed in the experimental spectra is analysed using the R-matrix with pseudo-states (RMPS) method. Results are also compared with the screening constant by unit nuclear charge (SCUNC) calculations. We characterize and identify the strong 1s $\rightarrow$ 2p resonances for both ions and the weaker 1s $\rightarrow$ *n*p resonances ($n \geq 3$) observed in the *K*-shell spectra of O^{4+}.

Key words: atomic data – atomic processes.

1 INTRODUCTION

The launch of the satellite *Astro-H* (renamed *Hitomi*) on 2016 February 17 was expected to provide X-ray spectra of unprecedented quality and would have required a wealth of atomic and molecular data on a range of collision processes to assist with the analysis of spectra from a variety of astrophysical objects. The subsequent break-up on 2016 March 28 of *Hitomi* now leaves a void in observational X-ray spectroscopy. In the intervening period before the launch of the next X-ray satellite mission, ground-based X-ray experiments along with theoretical cross-sections will continue to be benchmarked against each other, in order to extend our data base of knowledge on astrophysically important ions of carbon, nitrogen and oxygen.

Measurements of cross-sections for the photoionization of atoms and ions are essential data for testing theoretical methods in fundamental atomic physics (Berkowitz 1979; West 2001; Kjeldsen et al. 2002; Müller 2015) and for modelling of many physical systems, for example, terrestrial plasmas, the upper atmosphere and a broad range of astrophysical objects (quasar stellar objects, the atmosphere of hot stars, protoplanetary nebulae, H II regions, novae and supernovae; Lee et al. 2001; Blustin et al. 2002, 2003; Kaastra et al. 2002, 2004; Juett, Schulz & Chakrabarty 2004; Pinto et al. 2013, 2014; Nicastro et al. 2016a,b).

X-ray spectroscopy of highly ionized atomic oxygen is used to probe the hot gaseous halo of the Milky Way (Gupta et al. 2012, 2014; Miller & Bergman 2015; Nicastro et al. 2016c). Multiple ionization stages of C, N, O, Ne and Fe have been observed in the ionized outflow in the planetary nebulae NGC 4051, and measured with the satellite *XMM–Newton* (Ogle et al. 2004; Pinto et al. 2013) in the soft-X-ray region. Low-ionized stages of C, N and O have also been used in the modelling of X-ray emission from OB supergiants (Cassinelli et al. 1981). Multiple ionization stages of O and Fe are also seen in the *XMM–Newton* spectra from the Seyfert galaxy NGC 3783, including ultraviolet (UV) imaging, X-ray and UV light curves, the 0.2–10 keV X-ray continuum, the iron *K*-emission line and high-resolution spectroscopy in the modelling of the soft X-ray warm absorber (Blustin et al. 2002, 2003; Krongold et al. 2003; Mendoza et al. 2012; Gatuzz et al. 2013a, 2014; Gorczyca et al. 2013). Limited-wavelength observations for X-ray transitions were recently made on atomic oxygen, neon and magnesium, and their ions with the High Energy Transmission Grating (HETG) on board the *Chandra* satellite (Liao, Zhang & Yao 2013). Strong absorption *K*-shell lines of atomic oxygen, in its various forms of ionization, have been observed by the *XMM–Newton* satellite in the interstellar medium, through X-ray

★ E-mail: bmclaughlin899@btinternet.com (BMM); jean-marc.bizau@u-psud.fr (JMB); mgharaibeh@qu.edu.qa (MFG)
† Previous address: Department of Physics, Jordan University of Science, Technology, Irbid 22110, Jordan.

© 2016 The Authors
Published by Oxford University Press on behalf of the Royal Astronomical Society

Downloaded from https://academic.oup.com/mnras/article/465/4/4690/2556152 by Qatar University user on 27 August 2024

spectroscopy of low-mass X-ray binaries (Pinto et al. 2013). The *Chandra* and *XMM–Newton* satellite observations may be used to identify absorption features in astrophysical sources, such as active galactic nucleus and X-ray binaries, and for assistance in benchmarking theoretical and experimental work (Gatuzz et al. 2013a,b; Gorczyca et al. 2013; McLaughlin et al. 2013b,a; Gatuzz et al. 2014; McLaughlin et al. 2014; Bizau et al. 2015).

To our knowledge, previous experimental and observational X-ray lines on Be-like and Li-like atomic oxygen ions are limited to the $1s \rightarrow np$ regions (where $n = 2$, 3, 4 and 5), i.e. the Kα, Kβ, Kγ and Kδ lines, in the vicinity of the *K*-shell region (Bruch et al. 1979, 1987; Hoffmann et al. 1990, 1991; Nicolosi & Tondello 1997; Lee et al. 2001; Kaastra et al. 2002, 2004; Behar et al. 2003; Schmidt et al. 2004; Gu et al. 2005; Yao et al. 2009; Mendoza et al. 2012; Ramírez 2013; Liao et al. 2013; Pinto et al. 2013, 2014; Cabot, Wang & Yao 2013; Nicastro et al. 2016a,b). Prior to the present *K*-shell investigations at the SOLEIL radiation facility on photoionization cross-sections and Auger resonance states along the atomic oxygen iso-nuclear sequence, a few experiments have been devoted to the study of *K*-shell photoionization of oxygen ions. Nicolosi & Tondello (1997) observed satellite lines of He-like and Li-like laser-produced plasmas of Be, B, C, N and O. Auger spectra of core-excited oxygen ions emitted in the collision of fast oxygen-ion beams with gas targets and foils were measured by Bruch and co-workers (Bruch et al. 1979, 1987). Hoffmann and co-workers (Hoffmann et al. 1990, 1991) measured Auger resonance energies in electron-impact ionization studies of Be-like and Li-like ions. *K*-shell X-ray lines from inner-shell excited and ionized ions of oxygen were observed using the Lawrence Livermore National Laboratory EBIT from O^{2+} to O^{5+} (Schmidt et al. 2004; Gu et al. 2005).

For the oxygen isonuclear sequence, theoretical data are available for the energies for *K*-shell Auger or radiative transitions. Resonance energies and linewidths for Auger transitions in Be-like (Bruch et al. 1979) and Li-like atomic ions (Piangos & Nicolaides 1993) have been calculated using a variety of methods such as $1/Z$ perturbation theory (Murakami, Safronova & Kato 2002), multiconfiguration Dirac–Fock (MCDF; Bruch et al. 1979; Chen 1985, 1986; Chen, Zhang & Gou 2006), the saddle-point method (SPM) with R-matrix (Davis & Chung 1985, 1989) and complex-coordinate rotation methods (Zhang & Yeager 2012a,b). We note that Moore (1993) made an assessment of the energy levels of carbon, nitrogen and oxygen atoms and their ions. Chen and co-workers calculated the Auger and radiative decay of 1s-vacancy states in the Be isoelectronic sequence using the MCDF approach (Chen 1985, 1986; Chen & Crasemann 1987b). Zhang & Yeager (2012b) used the SPM with rotation (Davis & Chung 1985; Bingcong & Wensheng 2000) to calculate energy levels and Auger decay widths for the $1s2s^22p\ ^{1,3}P^o$ levels in a Be-like system. The recent saddle-point with rotation calculations by Yeager and co-workers (Zhang & Yeager 2012b), for resonance energies and Auger decay rates, for the $1s2s^22p\ ^1P^o$ levels in Be-like carbon showed an excellent agreement with previous measurements made at the Advanced Light Source (ALS) and R-matrix calculations (Scully et al. 2005).

In the case of Be-like and Li-like atomic oxygen systems, state-of-the-art *ab initio* photoionization cross-sections, resonance energies and decay rates for Auger inner-shell processes were calculated by Pradhan and co-workers (Pradhan 2000; Nahar, Pradhan & Zhang 2001; Pradhan et al. 2003) using the R-matrix method. Garcia and co-workers (Garcia et al. 2005) extended this work using the R-matrix optical potential method within an intermediate-coupling scheme (Burke 2011) to account for the Auger broadening of the resonances in the near *K*-edge region. Photoionization from the ground state, along the oxygen isonuclear sequence, was investigated in the photon energy region of the *K*-edge for both Be-like and Li-like atomic oxygen ions.

In this study, we focus our attention on obtaining detailed spectra for Be-like [O^{4+} (O V)] and Li-like [O^{5+} (O VI)] atomic oxygen ions in the vicinity of the *K*-edge. This work is the completion of photoionization cross-section measurements and theoretical studies along the atomic oxygen isonuclear sequence. Our previous studies on this sequence focused on obtaining photoionization cross-sections for the O^+ and O^{2+} ions (Bizau et al. 2015) and the O^{3+} ion (McLaughlin et al. 2014), where differences of 0.5 eV in the positions of the Kα resonance lines with prior satellite observations were found. This will have major implications for astrophysical modelling.

2 EXPERIMENT

2.1 Ion production

The measurements were made using the Multi-Analysis Ion Apparatus merged-beam set-up on the PLEIADES photon beam line at SOLEIL, the French synchrotron radiation (SR) facility. The set-up and the experimental procedure have been described previously in detail (Bizau et al. 2016), and we will give only the characteristics of relevance for the present experiment. The oxygen ion beams are produced in a permanent magnet electron cyclotron resonance ion source (ECRIS). Oxygen gas introduced in the ECRIS chamber is heated by a 12.6 GHz radio wave at a power of approximately 25 W. A constant 4 kV bias is applied on the source to extract the ions. They are selected in mass/charge ratio by a dipole magnet before being collimated and merged with the photon beam in the 60-cm-long interaction region. A second dipole magnet analyses the charge state of the ions after interaction with the photons. The parent ions are collected in a Faraday cup, while the photoions (the ions that have increased in charge state by 1 in the interaction) are counted using channel plates.

2.2 Excitation source

The photon beam is the SR emitted by the Apple II undulator of the PLEIADES beam line. The light is monochromatized using a 600 l mm^{-1} high flux grating. In the energy range considered in this work, the spectral purity is achieved by a cut-off of the mirror transmission and the use of a varied groove depth for the grating. The photon energy is determined using an ionization chamber (Samson 1967). For this work, we used for calibration purposes an energy of 539.17 $\pm$ 0.15 eV for the O_2 $1s \rightarrow 3s\sigma$ transition, as determined in Bizau et al. (2015). The photon energy is corrected for the Doppler shift produced by the two counter-propagating beams.

2.3 Experimental procedure

The absolute photoionization cross-sections σ are obtained at a given photon energy using the procedure previously described in Bizau et al. (2016) from the relation

$$\sigma = \frac{Se^2\eta\nu q}{IJ\epsilon \int_0^L \frac{dz}{\Delta x \Delta y F(z)}}. \quad (1)$$

The photoions counting rate S is corrected from the spurious ion signal produced by collisional-ionization processes using a chopper

Downloaded from https://academic.oup.com/mnras/article/465/4/4690/2556152 by Qatar University user on 27 August 2024

Table 1. Typical values for the experimental parameters involved in evaluating the absolute O^{4+} cross-section measured at a photon energy of 554.25 eV.

S	540 Hz
Noise	150 Hz
ν	5.4×10^5 m s^{-1}
Photon flux	5.1×10^{12} s^{-1}
J	50 nA
ϵ	0.92
F_{xy}	5.9×10^4 m^{-1}

placed at the exit of the photon beam line. In equation (1), ν is the velocity in the interaction region of the target ions of charge state q, I is the current produced by the photons on an SXUV300 IRD photodiode of efficiency η calibrated at the Physikalisch-Technische Bundesanstalt beam line at BESSY in Berlin, J is the current of incident ions, and ϵ is the efficiency of the microchannel plates. $\Delta x \Delta y F(z)$ is an effective beam area (with z the propagation axis of the two beams), where F is the two-dimensional form factor determined using three sets of xy slit scanners placed at each end and in the middle of the interaction region. The length L of the interaction region is fixed by applying a -1 kV bias on the tube delimiting the interaction region. The bias discriminates the photoions produced inside and outside the tube due to their different velocities. Typical values of the parameters involved in equation (1), measured for the O^{4+} target ion at a photon energy of 554.25 eV, are given in Table 1. The cross-section accuracy is determined by the statistical fluctuations on the photoion and background counting rates, plus a systematic contribution resulting from the measurement of the different parameters in equation (1). The latter is estimated to be 15 per cent and is dominated by the uncertainty on the determination of the photon flux and the form factor. Two modes are used for the acquisition of the cross-sections. One with no bias applied to the interaction tube, allowing us to determine with higher statistics and spectral resolution the relative cross-sections, which are latter normalized on the absolute cross-sections obtained in the second mode with the voltage applied to the interaction tube.

3 THEORY

3.1 SCUNC: Li-like and Be-like nitrogen

Previously, we used the Screening Constant by Unit Nuclear Charge (SCUNC) method in our theoretical work for O^{3+} (McLaughlin et al. 2014) to provide energies and Auger decay rates to complement our detailed *ab initio* calculations. The basic equations used to determine the resonance energy positions and the Auger widths are summarized here for completeness.

In the SCUNC formalism (Sakho 2011, 2012; Sakho et al. 2013), one has the total energy of the core-excited states given by

$$E\left(N\ell n\ell';^{2S+1}L^{\pi}\right) = -Z^2\left[\frac{1}{N^2} + \frac{1}{n^2}(1-\beta)^2\right], \quad (2)$$

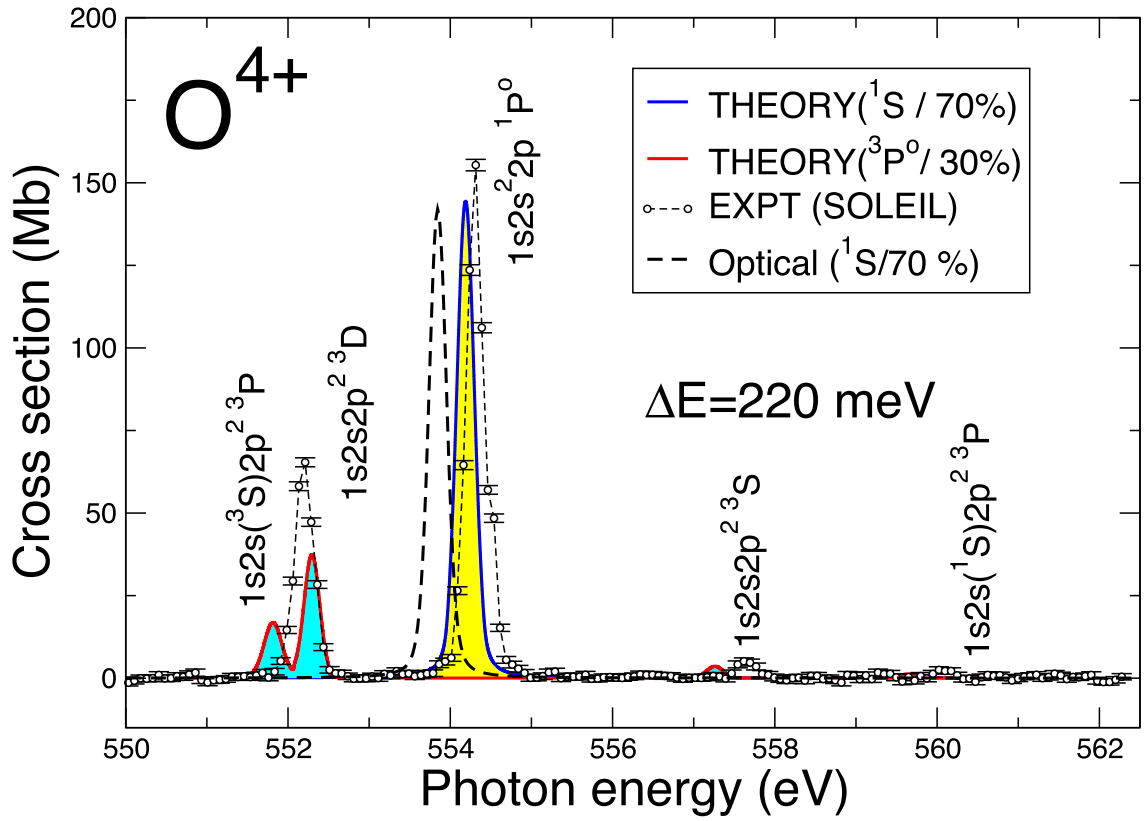

Figure 1. SOLEIL experimental K-shell photoionization cross-section of O^{4+} ions in the 550–562 eV photon energy range. Measurements were made with a 220 meV band-pass at FWHM. Solid points are experiment: The error bars represent the statistical uncertainty. Solid lines are the RMPS calculations for the ground (solid blue line) and metastable states (solid red line) with an appropriate admixture (see text for details). Dashed line (black) is the intermediate coupling R-matrix calculations (Garcia et al. 2005), for the ground state only, using the optical potential method. The strong 1s → 2p resonances are clearly visible in the spectra. The resonance parameters are presented in Table 2 and compared with previous work in the literature. [A colour version of this figure is available in the online version.]

Downloaded from https://academic.oup.com/mnras/article/465/4/4690/2556152 by Qatar University user on 27 August 2024

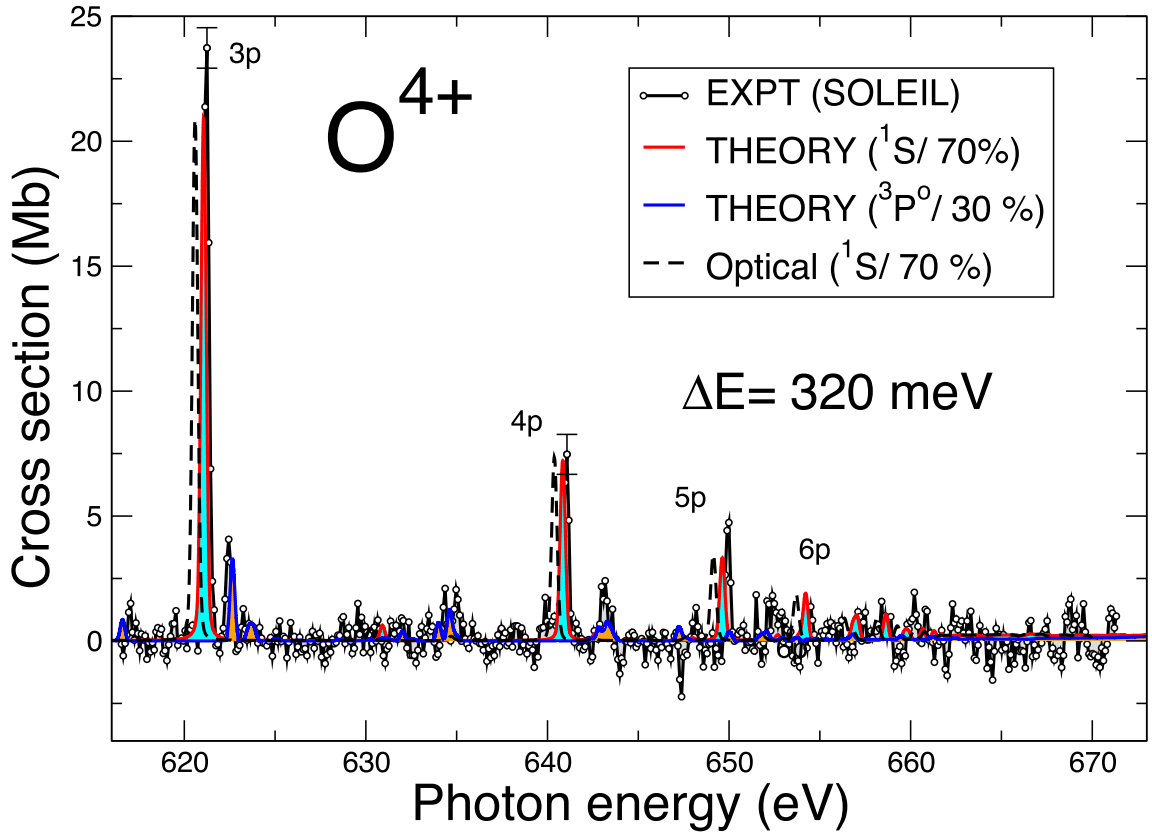

Figure 2. SOLEIL experimental *K*-shell photoionization cross-section of O^{4+} ions in the 615–672 eV photon energy range. Measurements were made with a 320 meV band-pass at FWHM. Solid points are experiment: The error bars represent the statistical uncertainty. The solid lines are the RMPS calculations with an appropriate admixture (see text for details). Dashed line (black) is the intermediate coupling R-matrix calculations (Garcia et al. 2005), for the ground state only, using the optical potential method. The strong 1s → *n*p resonances associated with the $1s^2 2s^2\ ^1S$ ground state are clearly visible in the spectra. The weaker features in the spectrum are from the $1s^2 2s2p\ ^3P^o$ metastable state. The resonance parameters are tabulated in Table 3. [A colour version of this figure is available in the online version.]

where $E(N\ell n\ell'; {}^{2S+1}L^{\pi})$ is in Rydberg units. In this equation, the principal quantum numbers N and n are, respectively, for the inner and the outer electrons of the He-like isoelectronic series. The β parameters are SCUNC expanded in inverse powers of Z and are given by the expression

$$\beta\left(N\ell n\ell'; {}^{2S+1}L^{\pi}\right) = \sum_{k=1}^{q} f_k \left(\frac{1}{Z}\right)^k, \tag{3}$$

where $f_k(N\ell n\ell'; {}^{2S+1}L^{\pi})$ are parameters to be evaluated empirically from previous experimental measurements. Similarly, one may get the Auger widths Γ in Rydbergs (1 Rydberg = 13.605 698 eV) from the formula

$$\Gamma(\mathrm{Ry}) = Z^2\left[1 - \frac{f_1}{Z}\left(\frac{Z}{Z_0} - \frac{1}{Z^2}\frac{(Z-Z_0)}{Z_0^2} - \frac{1}{Z^3}\frac{(Z-Z_0)}{Z_0^3}\right)\right]^2. \tag{4}$$

The measurements of Müller and co-workers on Be-like boron and carbon, and Li-like boron and carbon (Scully et al. 2005; Müller et al. 2009, 2010, 2014) were used to determine all the appropriate empirical parameters used in this work.

3.2 R-matrix with pseudo-states

The RMPS method (Mitnik et al. 1999; Burke 2011) was used to calculate the inner-shell photoionization cross-sections for the atomic oxygen ions, O^{4+} and O^{5+}, in their respective *K*-shell energy regions. The RMPS method (Mitnik et al. 1999; Burke 2011), using an efficient parallel implementation of the codes (Ballance & Griffin 2006; McLaughlin & Ballance 2015; McLaughlin et al. 2015, 2016, 2017), was used to determine all the cross-sections presented here.

Two different basis sets and scattering models were used only in our investigations on the O^{5+} ion. In the first collision model, we used Slater orbitals, where the $n = 3$ physical and $\overline{n} = 4$ pseudo-orbitals were used for the residual atomic oxygen ion, O^{6+}, in the *K*-shell energy region. This basis we designate as basis set A. All the Slater orbitals were generated using the CIV3 structure code (Hibbert 1975).

In the case of O^{5+} ion photoionization, 17-levels in *LS* (orbital and spin momentum) coupling and 31-levels in intermediate coupling were incorporated in our close-coupling approximation for the residual O^{6+} ion, where semi-relativistic effects were included [through the Breit–Pauli (BP) approximation]. These intermediate-coupling BP photoionization cross-section calculations were performed in order to gauge the influence of relativistic effects on resonance positions, profiles and widths for this Li-like system.

In the second approach, we used the AUTOSTRUCTURE code (Badnell 1986, 2011) to generate the target-wave functions for the subsequent photoionization cross-section calculations for both these ions. This we designate as basis set B. For each of the atomic oxygen ions, O^{4+} and O^{5+}, physical orbitals up to $n = 3$ were employed.

Downloaded from https://academic.oup.com/mnras/article/465/4/4690/2556152 by Qatar University user on 27 August 2024

Table 2. Be-like atomic oxygen ions, 1s → 2p excitation from the $1s^22s^2[^1S] \rightarrow 1s2s^22p[^1P^o]$ and $1s^22s2p[^3P^\circ] \rightarrow 1s2s2p^2[^3D,^3P,^3S]$ core-excited states. Comparison of experimental, satellite observational and theoretical resonance energies $E_{ph}^{(res)}$ (eV), natural linewidths Γ (meV) and resonance strengths $\overline{\sigma}^{PI}$ (Mb eV), for the photoexcited $n = 2$ states of the O^{4+} ion, in the photon energy region of 550–562 eV. The SOLEIL experimental determination of the resonance energy gives the uncertainty relative to line 2. For the total uncertainty, add 0.15 eV. For the conversion of the satellite wavelength observations to the present energy scale, $hc = 1239.841\ 974$ eV nm and the absolute error $\Delta E = hc\Delta\lambda/\lambda^2$ in eV were used.

Resonance (label)		SOLEIL (other experiments)	Satellite (observation)	R-matrix (theory)	MCDF (theory)	Others (theory)
$1s^22s2p[^3P^\circ] \rightarrow 1s2s[^3S]2p^2\ ^3P$	$E_{ph}^{(res)}$	–	$550.063^{+0.46\,m}_{-0.46}$	551.816[a]	550.200[d]	551.875[r]
					550.172[d]	552.884[s]
(0)						551.995[t]
	Γ	–		73[a]	23[d]	13[t]
	$\overline{\sigma}^{PI}$	–		4.9[a]		
$1s^22s2p[^3P^\circ] \rightarrow 1s2s2p^2\ ^3D$	$E_{ph}^{(res)}$	552.130 ± 0.03[h]	$551.016^{+0.64\,m}_{-0.64}$	552.296[a]	551.100[d]	552.736[r]
		552.030 ± 0.80[k]			551.175[d]	553.131[s]
(1)						552.432[t]
	Γ	44 ± 6[h]		42[a]	62[d]	59[t]
	$\overline{\sigma}^{PI}$	19.8 ± 3[h]		9.2[a]		
$1s^22s^2[^1S] \rightarrow 1s2s^22p\ ^1P^\circ$	$E_{ph}^{(res)}$	554.250 ± 0.00[h]	$554.079^{+0.42\,m}_{-0.42}$	554.189[a]	553.150[d]	552.287[e]
		554.243 ± 0.24[i]	$553.996^{+0.25\,n}_{-0.25}$	554.550[b]	553.241[d]	553.071[f]
(2)		554.144 ± 0.07[j]		554.739[c']	553.117[d]	553.971[r]
		554.370 ± 0.20[l]		553.853[g]		554.243[s]
						554.796[t]
						554.288[u]
	Γ	72 ± 4[h]		66[a]	58[d]	72[e]
				63[c]		62[f]
				66[g]		84[t]
	$\overline{\sigma}^{PI}$	49 ± 7[h]		43[a]		
				44[g]		
$1s^22s2p[^3P^\circ] \rightarrow 1s2s2p^2\ ^3S$	$E_{ph}^{(res)}$	557.690 ± 0.05[h]	$556.757^{+0.53\,m}_{-0.53}$	557.262[a]	556.500[d]	557.508[r]
			$556.330^{+0.10\,o}_{-0.10}$		556.494[d]	558.563[s]
			$556.050^{+0.70\,p}_{-0.70}$			
(3)			$556.732^{+0.50\,q}_{-0.50}$			557.798[t]
	Γ	–		40[a]	31[d]	
	$\overline{\sigma}^{PI}$	2.3 ± 0.3[h]		0.98[a]		
$1s^22s2p[^3P^\circ] \rightarrow 1s2s[^1S]2p^2\ ^3P$	$E_{ph}^{(res)}$	560.060 ± 0.07[h]		559.657[a]	560.020[d]	560.203[r]
					560.013[d]	561.243[s]
(4)						
	Γ	–		74[a]	66[d]	
	$\overline{\sigma}^{PI}$	0.6 ± 0.1[h]		0.3[a]		

Notes. [a]RMPS, 526-levels, basis B.
[b]R-matrix (Berrington, Quigley & Zhang 1997).
[c]R-matrix (Petrini & Tully 1991).
[c']R-matrix (Pradhan et al. 2003).
[d]MCDF (Chen 1985, 1986; Chen & Crasemann 1987b).
[e]Complex-scaled multireference configuration interaction (CMR-CI) (Zhang & Yeager 2012b).
[f]Saddle point + complex rotation (SPCR; Lin, Hsue & Chung 2001).
[g]R-matrix optical potential (Garcia et al. 2005).
[h]SOLEIL (present work). [i]EBIT (Gu et al. 2005).
[j]EBIT (Schmidt et al. 2004).
[k]Electron impact ionization (Hoffmann et al. 1990).
[l]AUGER spectroscopy (Bruch et al. 1987).
[m]*Chandra* observations in Mrn 279 (Kaastra et al. 2004).
[n]*Chandra* observations in NGC 5548 (Kaastra, private communication; Schmidt et al. 2004).
[o]*Chandra* observations (Liao et al. 2013).
[p]*Chandra* observations (Mendoza et al. 2012).
[q]*XMM –Newton* observations (Blustin et al. 2002).
[r]COWAN code (Kaastra et al. 2004).
[s]HULLAC code (Kaastra et al. 2004).
[t]SCUNC (present work; see text for details).
[u]FAC code Gu (2010) private communication (Liao et al. 2013).

Downloaded from https://academic.oup.com/mnras/article/465/4/4690/2556152 by Qatar University user on 27 August 2024

Table 3. Be-like atomic oxygen ions, $1s \rightarrow np$ excitation from the $1s^2 2s^2[^1S] \rightarrow 1s2s^2np[^1P^o]$ and $1s^2 2s2p[^3P^\circ] \rightarrow 1s2s2pnp[^3D, ^3P, ^3S]$ ($n > 2$) core-excited states. Comparison of experimental, satellite observational and theoretical resonance energies $E_{ph}^{(res)}$ (eV), natural linewidths Γ (meV) and resonance strengths $\overline{\sigma}^{PI}$ (Mb eV), for the photoexcited states of the O^{4+} ion, in the photon energy region of 615–675 eV. The SOLEIL experimental determination of the resonance energy gives the uncertainty relative to line 2. For the total uncertainty, add 0.15 eV. For the conversion of the satellite wavelength observations into the present energy scale, $hc = 1239.841\,974$ eV nm and the absolute error $\Delta E = hc\Delta\lambda/\lambda^2$ in eV were used.

Resonance (label)		SOLEIL (other experiments)	Satellite (observation)	R-matrix (theory)	MCDF[c] (theory)	Others (theory)
$1s^2 2s^2[^1S] \rightarrow 1s2s^2 3p\,^1P^\circ$ (5)	$E_{ph}^{(res)}$	621.230 ± 0.05^e	–	621.063^a 620.604^b	–	622.137^f
	Γ	–		80^a 54^b		94^f
	$\overline{\sigma}^{PI}$	8.6 ± 1.3^e		8.4^a 8.3^b		
Resonance (6)	$E_{ph}^{(res)}$	622.440 ± 0.07^e	–	622.653^a	–	
	Γ	–		11^a		
	$\overline{\sigma}^{PI}$	1.4 ± 0.2^e		1.1^a		
$1s^2 2s^2[^1S] \rightarrow 1s2s^2 4p\,^1P^\circ$ (7)	$E_{ph}^{(res)}$	641.040 ± 0.06^e	$641.408^{+0.55}_{-0.55}{}^d$	640.841^a 640.388^b	–	641.852^f
	Γ	–		78^a 52^b		67^f
	$\overline{\sigma}^{PI}$	3.6 ± 0.5^e		2.9^a 3^b		
Resonance (8)	$E_{ph}^{(res)}$	643.120 ± 0.09^e	–	643.273^a	–	–
	Γ	–		7^a		
	$\overline{\sigma}^{PI}$	1.2 ± 0.2^e		0.2^a		
$1s^2 2s^2[^1S] \rightarrow 1s2s^2 5p\,^1P^\circ$ (9)	$E_{ph}^{(res)}$	649.940 ± 0.07^e	$650.494^{+0.56}_{-0.56}{}^d$	649.630^a 649.143^b	–	650.978^f
	Γ	–		78^a 55^b		48^f
	$\overline{\sigma}^{PI}$	2.7 ± 0.4^d		1.4^a 1.4^b		

Notes. [a]RMPS, 526-levels, basis B.
[b]R-matrix optical potential (Garcia et al. 2005).
[c]MCDF (Chen 1985, 1986; Chen & Crasemann 1987b).
[d]*XMM–Newton* observations in NGC 3783 (Behar et al. 2003).
[e]SOLEIL (present work).
[f]SCUNC (present work; see text for details).

These were augmented with correlation-type orbitals $\bar{n}\ell = 4\bar{\ell}, \ldots, 14\bar{\ell}$, where $\ell = 0$, 1, 2, 3 and 4, i.e. s, p, d, f and g, which are Laguerre-type pseudo-states. All the computations were performed in *LS* coupling. In this approach, we used 526-levels in our collision model for the residual O^{5+} ion for the photoionization of O^{4+}. In the case of *K*-shell O^{5+} photoionization, a collision model was utilized, which incorporated 120-levels of the residual O^{6+} ion in the close-coupling approximation.

3.3 Be-like atomic oxygen ions

For the O^{4+} ion, we used the RMPS method to perform all the photoionization cross-section calculations. All the photoionization cross-section calculations were performed in *LS* coupling. We note that the ion beam in the SOLEIL experiments contains both ground states and metastable states. Photoionization cross-section calculations were carried out for both these initial states of O^{4+}: $1s^2 2s^2\,^1S$ ground state and $1s^2 2s2p\,^3P^\circ$ metastable state. Thirty-five continuum orbitals were utilized in the collision calculations. In our collision model, we retained 526-levels in the close-coupling expansion, and basis set B was utilized for this scattering approximation. A boundary radius of 13.838 Bohr was required to cater to the very diffuse pseudo-states. In the outer region, we used an energy mesh of 1.36 μeV to fully resolve all the fine resonance features in the cross-sections.

3.4 Li-like atomic oxygen ions

For the O^{5+} ion, we used the RMPS method and the BP approximation to perform all the photoionization cross-sections. Basis set A was used with 17-levels included in *LS*-coupling and 31-levels in the intermediate-coupling approximations for the residual O^{6+} ion. In the SOLEIL measurements, for this ion, only the ground state is present, so cross-section calculations were performed for the $1s^2 2s\,^2S$ ground state of O^{5+} in *LS* coupling and in intermediate coupling, taking into account relativistic effects through the BP approximation.

Thirty-five continuum orbitals were utilized in the collision calculations and a boundary radius of 6.0 Bohr to accommodate the diffuse $n = 4$ orbitals for basis A. For the RMPS approach, 120-levels were retained in the close-coupling approximation, with basis set B. A boundary radius of 11.925 Bohr was required to cater to

Downloaded from https://academic.oup.com/mnras/article/465/4/4690/2556152 by Qatar University user on 27 August 2024

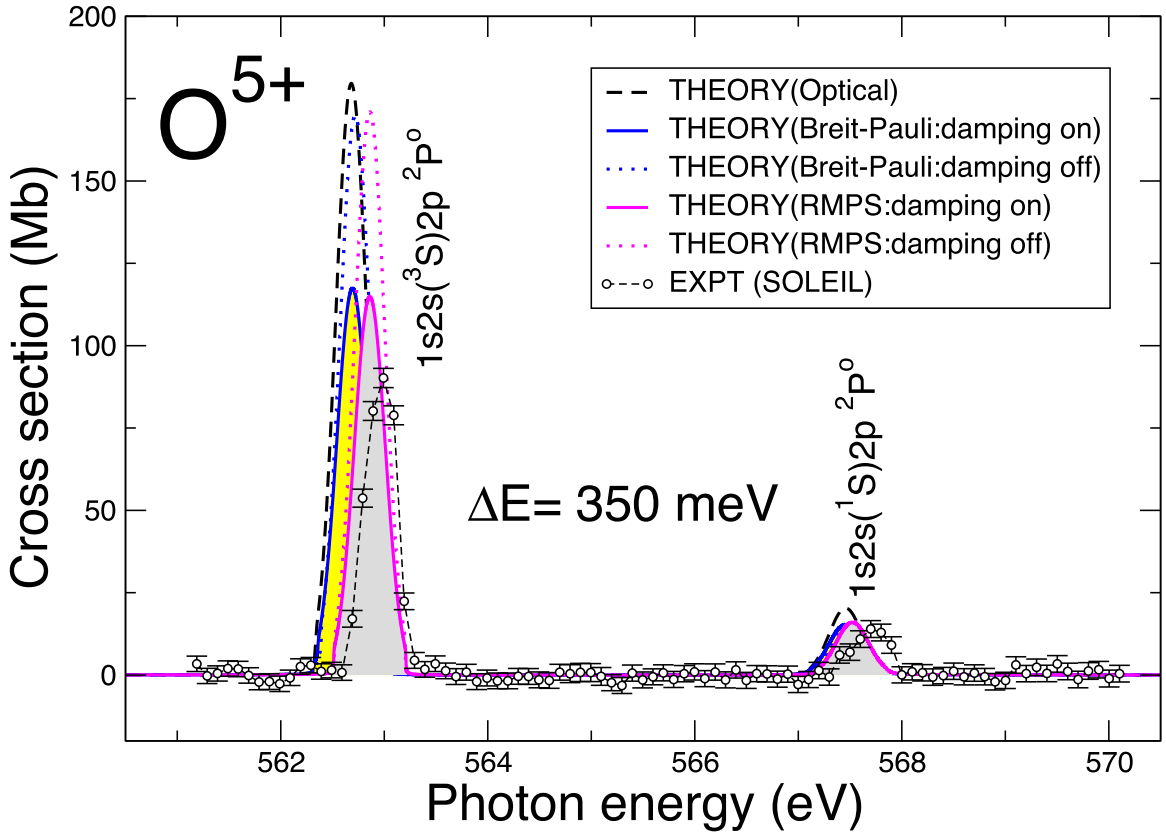

Figure 3. SOLEIL experimental *K*-shell photoionization cross-section of O^{5+} ions in the 561–570 eV photon energy range. Measurements were made with a 350 meV band-pass. Solid points are experiment: The error bars give the statistical uncertainty. The dashed (black) lines are the intermediate coupling (BP) calculations using the optical potential method (Garcia et al. 2005). The solid (magenta) line shows the present RMPS results, and the solid (blue) line shows the results from the BP approximation, both of which include radiation damping (Robicheaux et al. 1995). The dotted magneta line and the dotted blue line are the RMPS and BP approximations without radiation damping, respectively. The strong 1s → 2p resonances are clearly visible in the spectra. All the resonance parameters are given in Table 4 and compared with previous work from the literature. [A colour version of this figure is available in the online version.]

the very diffuse pseudo-states, and 35 continuum orbitals were used for the collision calculations.

Photoionization cross-section calculations for O^{5+} ions were performed both in *LS* coupling and in intermediate coupling. The intermediate-coupling calculations were carried out using the semirelativistic BP approximation, which allows for relativistic effects to be included. Radiation-damping (Robicheaux et al. 1995) effects were also included within the confines of the R-matrix approach (Burke 2011) for completeness as this affects only narrow resonances found in cross-sections for highly charged systems. For the O^{5+} ion, an energy mesh of 680 μeV resolved all the resonance features in the spectra for the photon energy range of 560–575 eV.

4 RESULTS AND DISCUSSION

Fig. 1 illustrates the experimental and theoretical results for the O^{4+} ion in the photon energy region of 550–562 eV, where the strong $1s \rightarrow 2p$ resonances are found. The theoretical cross-sections were convoluted with an appropriate Gaussian profile having a similar band width to the SOLEIL measurements: 220 meV for the region 550–565 eV. An admixture of the ground and metastable states was applied to simulate experiment. We found that 70 per cent of the $1s^22s^2\ ^1S$ ground and 30 per cent of the $1s^22s2p\ ^3P^o$ metastable states suitably matched theory with experiment. In Fig. 2, we present the photon energy region 615–670 eV, where the $1s \rightarrow np$ resonance features are located. Here again a similar admixture (70 per cent ground state and 30 per cent metastable state) for the theoretical cross-sections, after convolution by a Gaussian profile with 320 meV full width at half-maximum (FWHM), simulates the experimental results very well. Tables 2 and 3 compare our experimental and theoretical results for the resonance parameters for this Be-like systems with other theoretical, experimental and satellite observations. Figs 1 and 2 include the intermediate-coupling calculations of Garcia and co-workers (Garcia et al. 2005) performed using the optical potential method (dashed black line) convolved by the Gaussian profiles and weighted by 70 per cent for the ground state only for completeness.

The results for the resonance strengths $\bar{\sigma}^{\rm PI}$ found in the O^{4+} spectra are presented in Tables 2 and 3, and the resonance strengths have been weighted by the 70 per cent and 30 per cent admixture for the ground and metastable states to compare directly with experiment.

For the O^{4+} ion, it should be noted that from a comparison of the experimental and R-matrix resonance strengths $\bar{\sigma}^{\rm PI}$ (see Figs 1 and 2), excellent agreement, particularly for the strong resonant features (due to the $1s^22s^2\ ^1S$ ground state), in the spectrum is achieved. It can be seen from Tables 2 and 3 that the agreement between experiment and theory for the weaker resonant features in the spectra of O^{4+} (due to the $1s^22s2p\ ^3P^o$ metastable) is not as good as the ground state. The weak resonances 6 and 8 in Table 3 (originating from the $1s^22s2p\ ^3P^o$ metastable state) may be

Downloaded from https://academic.oup.com/mnras/article/465/4/4690/2556152 by Qatar University user on 27 August 2024

Table 4. Li-like atomic oxygen ions, 1s → 2p excitation from the $1s^2 2s[^2S] \rightarrow 1s(2s2p\,^1P^\circ)\,[^2P^o]$ and $1s(2s2p\,^3P^\circ)\,[^2P^\circ]$ core-excited states. Comparison of experimental, satellite observational and theoretical results for the resonance energies $E_{ph}^{(res)}$ (eV), natural linewidths Γ (meV) and resonance strengths $\overline{\sigma}^{PI}$ (Mb eV), for the photo-excited $n = 2$ states of the O^{5+} ion, in the photon energy region of 560–570 eV, with previous investigations. The uncertainty of the SOLEIL experiment energy of the lines is relative to line A. For the total uncertainty, add 0.15 eV for energy calibration. For the conversion of the satellite wavelength observations into the present energy scale, $hc = 1239.841\,974$ eV nm and the absolute error $\Delta E = hc\Delta\lambda/\lambda^2$ in eV were used.

Resonance (label)		SOLEIL (other experiments)	Satellite (observation)	R-matrix (theory)	MCDF (theory)	Others (theory)
$1s^2 2s[^2S] \rightarrow 1s(2s2p\,^3P^\circ)\,[^2P^\circ]$	$E_{ph}^{(res)}$	562.940 ± 0.00^{j}	$562.662^{+0.70\,q}_{-0.70}$	562.860^{a}	562.018^{d}	562.829^{e}
		563.000 ± 1.00^{k}	$562.899^{+0.10\,r}_{-0.10}$	$562.709^{a'}$	563.039^{d}	562.415^{f}
		563.119 ± 0.20^{n}	$562.950^{+0.08\,s}_{-0.08}$	562.297^{b}	562.803^{d}	563.440^{g}
(A)		563.068 ± 0.04^{o}	$562.828^{+0.06\,t}_{-0.05}$	562.680^{c}		563.057^{h}
		563.053 ± 0.15^{p}	$563.309^{+0.26\,u}_{-0.26}$			562.534^{x}
		563.100 ± 0.20^{m}	$562.287^{+0.40\,v}_{-0.40}$			$562.705^{i'}$
			$562.465^{+0.10\,y}_{-0.10}$			
			$562.912^{+0.24\,z}_{-0.23}$			
			$563.053^{+0.51\,z'}_{-0.51}$			
	Γ	–	6^{a}		5^{d}	6^{e}
				$6^{a'}$		4^{f}
				4^{b}		6^{g}
				9^{c}		$6^{i'}$
	$\overline{\sigma}^{PI}$	36 ± 5^{j}		42.52^{a}		
				$42.52^{a'}$		
				71.3^{c}		
$1s^2 2s[^2S] \rightarrow 1s(2s2p\,^1P^\circ)\,[^2P^\circ]$	$E_{ph}^{(res)}$	567.620 ± 0.05^{j}	$566.915^{+0.40\,v}_{-0.40}$	567.519^{a}	568.499^{d}	567.420^{e}
		566.081 ± 0.12^{l}		$567.445^{a'}$		567.420^{f}
(B)		567.719 ± 2.00^{m}		566.987^{b}		568.117^{g}
		568.000 ± 2.00^{n}		567.450^{c}		567.783^{i}
		567.563 ± 0.26^{p}				$567.762^{i'}$
	Γ	–		46^{a}	49^{d}	46^{f}
				$46^{a'}$		50^{g}
				45^{b}		45^{i}
				48^{c}		$59^{i'}$
	$\overline{\sigma}^{PI}$	7.4 ± 1^{j}		6.4^{a}		
				$6.3^{a'}$		
				8.6^{c}		

Notes. [a]RMPS, 120-levels, basis B.
[a′]R-matrix, BP, 31-levels, basis A.
[b]R-matrix (Pradhan et al. 2003).
[c]R-matrix, optical potential method, intermediate coupling (Garcia et al. 2005).
[d]MCDF (Chen 1985, 1986; Chen & Crasemann 1987a).
[e]Complex-scaled multireference configuration interaction (CMR-CI) (Zhang & Yeager 2012a).
[f]Saddle point + complex rotation (SPCR; Bingcong & Wensheng 2000).
[g]Saddle point + complex rotation (SPCR; Wu & Xi 1991).
[h]Intermediate coupling (Gabriel 1972).
[i]SPM (Davis & Chung 1989).
[i′]SCUNC (present work; see text for details).
[j]SOLEIL (present work).
[k]Auger spectroscopy (Bruch et al. 1979).
[l]EBIT (Gu et al. 2005).
[m]Auger spectroscopy (Bruch et al. 1987).
[n]Electron-impact ionization experiments (Hoffmann et al. 1990)
[o]EBIT (Schmidt et al. 2004).
[p]Laser plasma experiment (Nicolosi & Tondello 1997).
[q]*Chandra* observations (Mendoza et al. 2012).
[r]*Chandra* observations (Yao et al. 2009).
[s]*Chandra* observations (Gatuzz et al. 2013a,b).
[t]*Chandra* observations (Liao et al. 2013).
[u]*Chandra* observations in NGC 5548 (Kaastra, private communication; Schmidt et al. 2004).
[v]*Chandra* observations in NGC 5548 (Kaastra et al. 2002).
[x]FAC code (Gu, private communication; Liao et al. 2013).
[y]*Chandra* observations in MCG-6-30-15 (Lee et al. 2001).
[z]*XMM–Newton* observations in Cyg X-2 (Cabot et al. 2013).
[z′]*XMM–Newton* observations in Mrn 501 RGS1 (Nicastro et al. 2016b).

Downloaded from https://academic.oup.com/mnras/article/465/4/4690/2556152 by Qatar University user on 27 August 2024

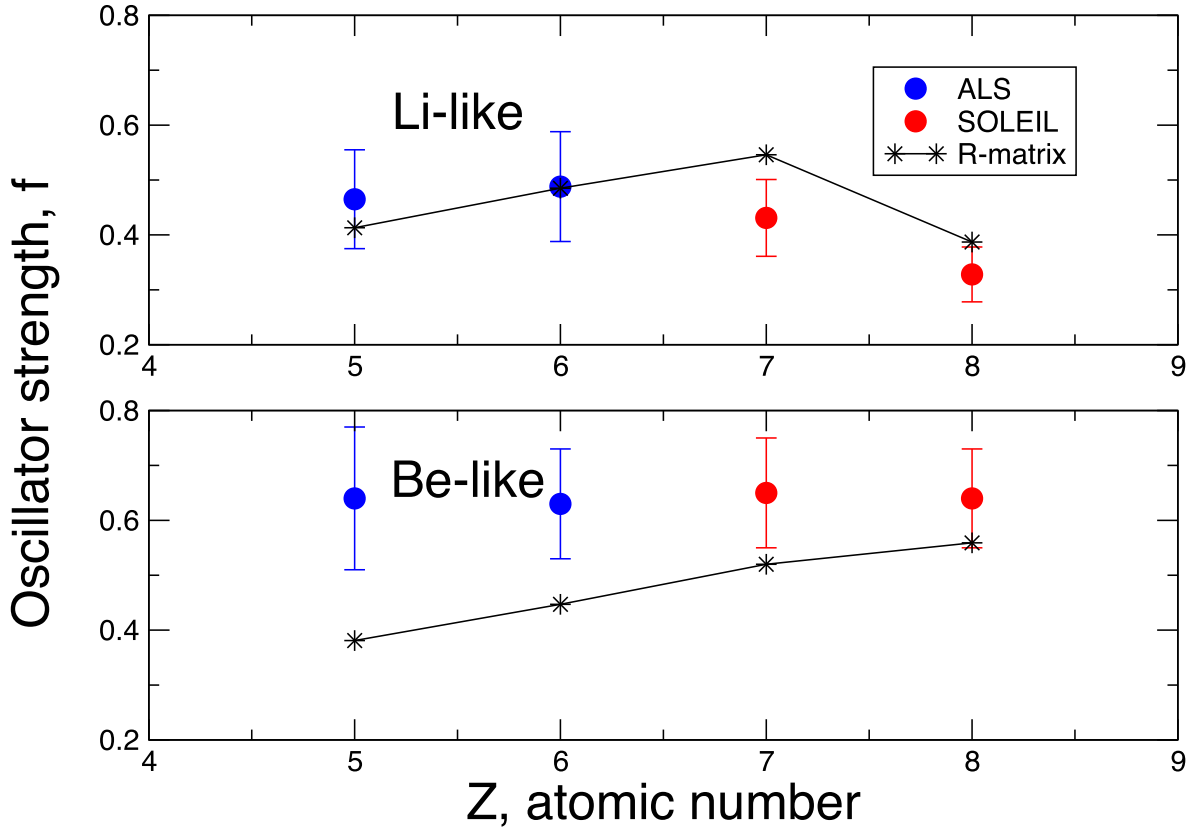

Figure 4. Comparison of the integrated oscillator strengths f obtained from SR measurements with R-matrix calculations. The solid circles are from the ALS (blue) and SOLEIL (red) radiation facilities for the Li-like and Be-like isoelectronic sequences. The asterisk values (black) are from R-matrix calculations. [A colour version of this figure is available in the online version.]

Table 5. Li-like and Be-like ions, integrated oscillator strength for the core-excited states arising from, respectively, the ground configurations $1s^2 2s$ and $1s^2 2s^2$ of each ion. The table shows a comparison of the present experimental and theoretical results for the integrated oscillator strengths f for the dominant core photoexcited $n = 2$ states of the first four ions of each sequence (Z is the atomic number of the ion) with previous investigations.

Z	Ion		Experiment	Theory
Li-like	$1s^2 2s\,^2S \rightarrow 1s[2s2p\,^3P]\,^2P^o$		Resonance	
5	B^{2+}	f	0.465 ± 0.09^a	$0.413^{a'}$
6	C^{3+}	f	0.483 ± 0.10^b	$0.485^{b'}$
7	N^{4+}	f	0.413 ± 0.07^c	0.546^i
8	O^{5+}	f	0.328 ± 0.05^d	0.387^j
Be-like	$1s^2 2s^2\,^1S \rightarrow 1s2s^2 2p\,^1P^o$		Resonance	
5	B^{+}	f	0.641 ± 0.13^e	0.413^g
6	C^{2+}	f	0.624 ± 0.10^f	0.447^h
7	N^{3+}	f	0.650 ± 0.10^c	0.546^i
8	O^{4+}	f	0.640 ± 0.09^d	0.559^j

Notes. [a]ALS, experiment (Müller et al. 2010).
[b]ALS, experiment (Müller et al. 2009).
[a′]R-matrix, theory (Müller et al. 2010).
[b′]R-matrix, theory (Müller et al. 2009)
[c]SOLEIL, experiment (Al Shorman et al. 2013).
[d]SOLEIL, experiment (present work).
[e]ALS, experiment (Müller et al. 2014).
[f]ALS, experiment (Scully et al. 2005).
[g]R-matrix, theory (Müller et al. 2014).
[h]R-matrix, theory (Scully et al. 2005).
[i]R-matrix, theory (Al Shorman et al. 2013).
[j]R-matrix, theory (present work).

identified with the aid of quantum defect theory. The weak resonance profiles of the remaining members of the Rydberg series emanating from the $1s^2 2s2p\ ^3P^o$ metastable state make them difficult to resolve experimentally.

Fig. 3 shows a comparison of the SOLEIL cross-section measurements made with a band-pass of 350 meV FWHM for the O^{5+} ion with our theoretical results, which include and exclude radiation damping (Robicheaux et al. 1995). In order to compare directly with experiment, theory has been convoluted with a Gaussian profile having a similar width of 350 meV at FWHM. The results from both the BP approximation (using basis A) and the RMPS method (using basis B) are shown. As seen from Fig. 3, the calculations of Garcia and co-workers (Garcia et al. 2005) performed (using the optical potential approach) in intermediate coupling would appear to not include radiation damping (Robicheaux et al. 1995), as they are similar to our BP results without radiation damping, and as such overestimate the resonance strength of the narrow resonance located by experiment at 562.94 eV. As illustrated in Fig. 3 and from the results presented in Table 4, the RMPS cross-sections (that include radiation damping) give the best agreement with the present measurements from the SOLEIL radiation facility for this ion in the photon energy region where the resonances of O^{5+} are located.

An additional check on the theoretical data is the comparison of the integrated oscillator strength f or the resonance strength with experiment. The quantity f for the theoretical and experimental spectra may be determined for each resonance using (Shore 1967; Fano & Cooper 1968; Berkowitz 1979)

$$f = 9.1075 \times 10^{-3} \bar{\sigma}^{\mathrm{PI}}. \quad (5)$$

Downloaded from https://academic.oup.com/mnras/article/465/4/4690/2556152 by Qatar University user on 27 August 2024

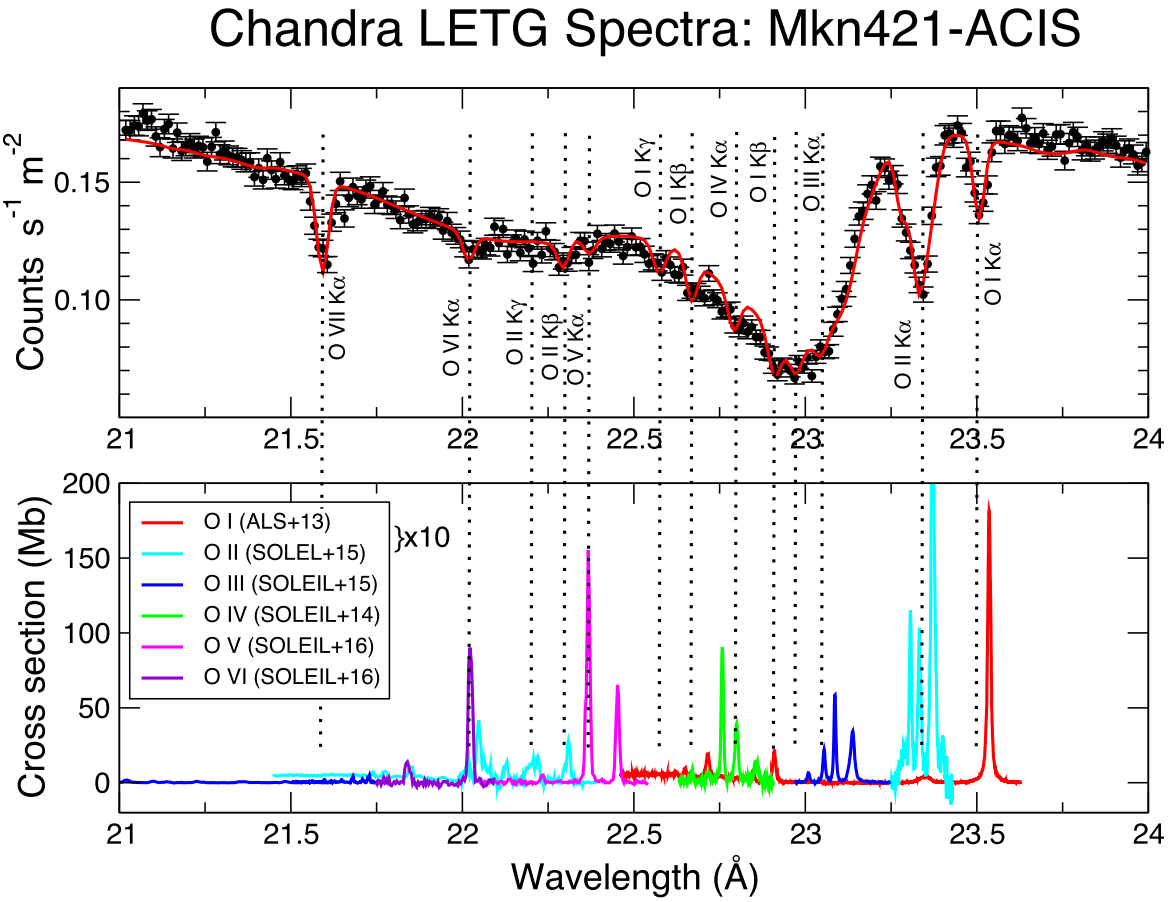

Figure 5. Top panel: *Chandra* LETG spectra for the blazar Mrk 421 ACIS in the wavelength range of 21–24 Å composed from several different exposures with the *Chandra* satellite (Nicastro et al. 2016a). Bottom panel: For the same wavelength range, measurements are illustrated from a combination of ground-based experimental spectra made at various SR facilities: ALS (O I) (McLaughlin et al. 2013a,b), SOLEIL (O II and O III) (Bizau et al. 2015), SOLEIL (O IV) (McLaughlin et al. 2014) and the present SOLEIL (O V and O VI) results. The strongest lines in the synchrotron measurements are from the ground state of each ionized stage of atomic oxygen. The weaker ones in the measurements are from the metastable states of each ionic complex. The O I and O II results are scaled by a factor of 10. [A colour version of this figure is available in the online version.]

The resonance strength in the photoionization cross-section $\bar{\sigma}^{\rm PI}$ is defined as

$$\bar{\sigma}^{\rm PI} = \int_{E_1}^{E_2} \sigma(h\nu)\mathrm{d}h\nu, \qquad (6)$$

where $[E_1, E_2]$ is the photon energy range over which each resonance profile extends.

Fig. 4 illustrates results for the oscillator strengths f along the Li-like and Be-like isoelectronic sequences, for the strong Kα transitions originating from the ground state of each ion. Table 5 tabulates these integrated oscillator strength f results obtained from SR measurements (ALS and SOLEIL) and those obtained from R-matrix calculations. For the Be-like sequence, the values have been corrected for ground-state populations. As can be seen from Table 5 and Fig. 4, apart from Be-like boron and to a lesser extent Be-like carbon, the agreement between theory and experiment along both isoelectronic sequences is quite satisfactory, giving further confidence in this work.

5 COMPARISON WITH SATELLITE OBSERVATIONS

In Tables 2–4, comparisons are made with the available experimental and satellite observations in the literature for resonance energies for Be-like and Li-like atomic oxygen ions. One can clearly see many discrepancies between our present ground-based measurements, made at SOLEIL, and the *Chandra* and *XMM–Newton* satellite observations. We note that for both atomic ions, the RMPS results favour those from the SOLEIL radiation facility.

Fig. 5 illustrates a comparison of various ground-based synchrotron cross-section measurements (ALS and SOLEIL) for the atomic oxygen isonuclear sequence in the wavelength region 21–24 Å with the low-energy-transmission-grating (LETG) spectra observed by *Chandra* for the blazar Mrk 421 ACIS (Nicastro et al. 2016a). One clearly sees, especially for low-charged stages of oxygen ions, discrepancies in the resonance energies for the strong Kα lines in the *Chandra* spectra compared to the different ground-based light source measurements which we discuss and quantify. The satellites observe O I to O IV lines (with a shift) and noshift in the O V and O VI lines, as seen in the comparison with the spectra for the blazar Mrk 421 (Nicastro et al. 2016a), shown in Fig. 5. Similar effects are also seen in the spectra of H 2356−309 LETG, H 2356−309 RGS1 and Mrk 501 RGS1, for the wavelength region 21–24 Å, in the recent observations of Nicastro and co-workers (Nicastro et al. 2016a,b). We note that similar differences are seen in the wavelength region 21–24 Å, for satellite observations in the high-energy-transmission grating (HETG)

Downloaded from https://academic.oup.com/mnras/article/465/4/4690/2556152 by Qatar University user on 27 August 2024

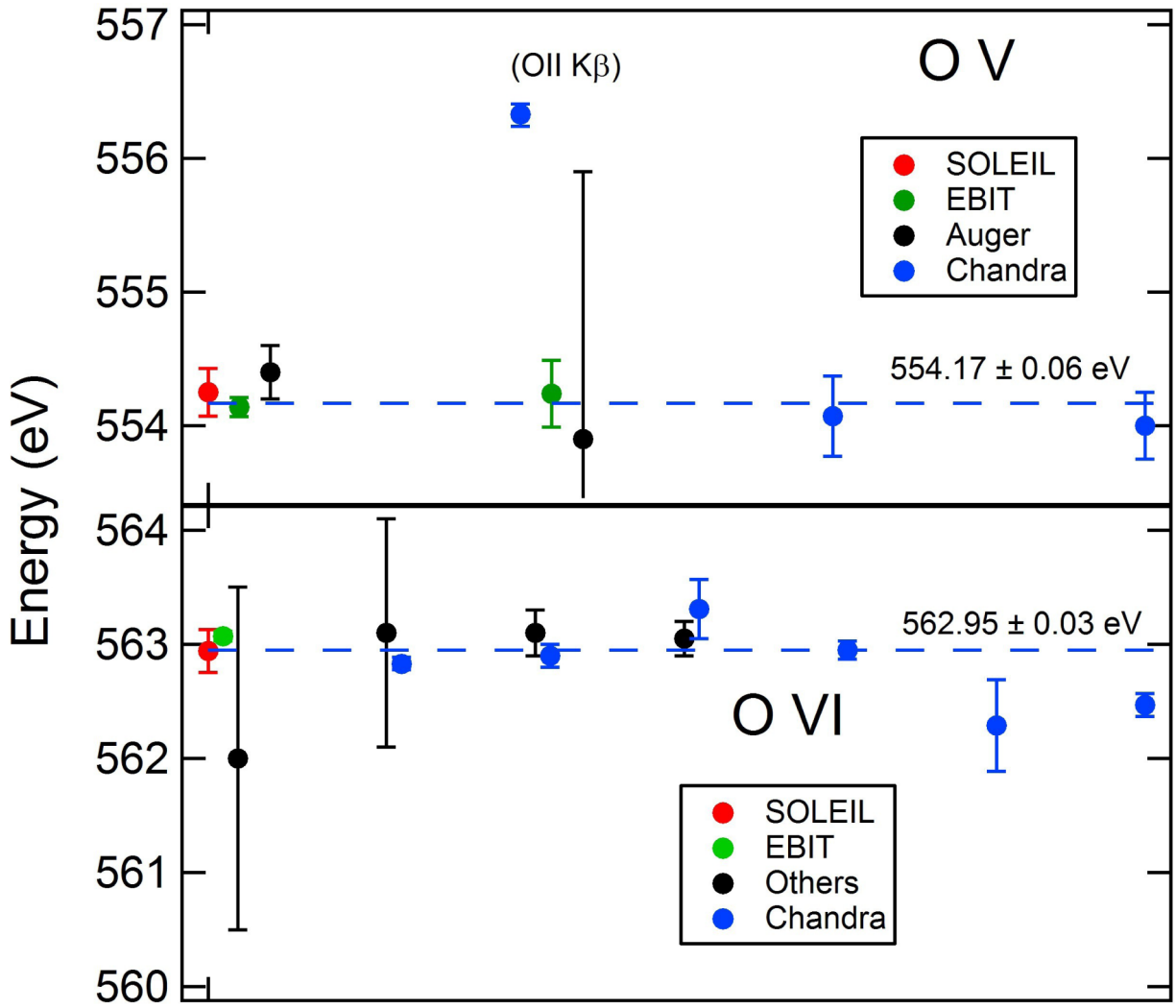

Figure 6. Top panel: comparison of the Kα energies for O^{4+} ions with values obtained from various experimental approaches, EBIT, Auger, the current SOLEIL measurements and *Chandra* observations. Bottom panel: similarly for the Kα energies for O^{5+} ions with various experimental and satellite observations with the current SOLEIL measurements. The dashed line (blue) in both panels is the ponderated mean of all the values. [A colour version of this figure is available in the online version.]

spectra observed by *Chandra* for the X-ray binary XTE J1817−332 (Gatuzz et al. 2013a,b), although no O IV or O V K lines are observed.

Fig. 6 illustrates more precisely the discrepancies for the O^{4+} and O^{5+} ions, Kα resonance lines between ground-based experiments and prior satellite observations. The present results are for the O^{4+}(O V) ion (top panel) and the O^{5+}(O VI) ion (bottom panel). Table 6 quantifies the differences between the ground-based experimental measurements (SR and EBIT) and the satellite observations (*Chandra* and *XMM–Newton*). We note in passing that the measurements performed at two independent ground-based light source experiments highlighted discrepancies in the energies of the Kα lines along the atomic oxygen isonuclear sequence compared to satellite observations. Furthermore, we point out that the *Chandra* observations of Liao et al. (2013), particularly for the O V line at 556.33 eV, appear to be a misidentification. This line is instead identified as the O II Kβ line. We have indicated this in Fig. 6. This misidentification was indicated in the observations of Gatuzz et al. (2014) and confirmed by the definitive observations of Nicastro et al. (2016a), who found the O II Kβ line at 556.482 ± 0.50 eV from the average of 29 X-ray sources.

The discrepancies with the satellite observations are as yet not fully understood (Kallman, private communication). We note that, for the synchrotron measurements, the energy calibration was originally based on EELS measurements of O_2 1s → π^* performed by Hitchcock & Brion (1980) and ion yield measurements of O_2 1s → 3σ by Tanaka et al. (2008). More recently, the energy calibration has been based on O_2 *K*-shell absorption spectra and photoelectron spectroscopy (PES) for 2s removal in neon (Bizau et al. 2015). As can clearly be seen from Table 7, the difference between the two types of energy calibrations is of the order of 0.22 eV, and therefore cannot account for the larger energy differences with the satellite observations. Further independent ground-based synchrotron light source measurements would be of great beneficial help to try and minimize this source of calibration error.

Downloaded from https://academic.oup.com/mnras/article/465/4/4690/2556152 by Qatar University user on 27 August 2024

Table 6. Comparison of the energies for the Kα resonance line (centroid in eV), ions in their ground state, along the atomic oxygen isonuclear sequence. The entries in the table are from SR light source and EBIT measurements, compared to available *Chandra* and *XMM–Newton* satellite observations. For the conversion of the satellite wavelength observations into the present energy scale, $hc = 1239.841\ 974$ eV nm was used.

Atomic oxygen	SR	EBIT		*Chandra* and *XMM*	
(ionized state)	E (eV)	E (eV)	ΔE (eV)	E (eV)	ΔE (eV)
O I	526.79(4)[a]			527.39(2)[g]	−0.60
				527.37(40)[o]	−0.58
				527.44(18)[p]	−0.65
O II	530.50(13)[b]			530.97(3)[g]	−0.47
				530.98(40)[o]	−0.48
O III	536.86(13)[b]	537.42(9)[e]	−0.55	537.94(2)[g]	−1.08
O IV	544.52(13)[c]	545.20(10)[e]	−0.68	546.22(8)[g]	−1.74
				546.43(24)[p]	−1.91
O V	554.25(18)[d]	554.14(7)[f]	0.11	556.33(9)[g,*]	−2.08
				554.00(25)[h]	−0.25
				554.08(42)[i]	0.17
O VI	562.94(18)[d]	563.07(4)[d]	−0.13	562.83(6)[g]	0.11
				562.90(10)[j]	0.04
				562.95(10)[k]	−0.01
				563.31(26)[h]	−0.63
				562.29(40)[l]	0.65
				562.47(10)[m]	0.47
				562.90(25)[n]	0.04
				563.05(51)[p]	−0.11

Notes. [a]ALS (McLaughlin et al. 2013a,b).
[b]SOLEIL (Bizau et al. 2015).
[c]SOLEIL (McLaughlin et al. 2014; Bizau et al. 2015).
[d]SOLEIL present results.
[e]EBIT (Gu et al. 2005).
[f]EBIT (Schmidt et al. 2004).
[g]*Chandra* (Liao et al. 2013).
[h]*Chandra* (Kaastra, private communication; Schmidt et al. 2004).
[i]*Chandra* (Kaastra et al. 2004).
[j]*Chandra* (Yao et al. 2009).
[k]*Chandra* (Gatuzz et al. 2013a,b).
[l]*Chandra* (Kaastra et al. 2002).
[m]*Chandra* (Lee et al. 2001).
[n]*XMM–Newton* (Cabot et al. 2013).
[o]*Chandra and XMM–Newton* (Nicastro et al. 2016a).
[p]*Chandra and XMM–Newton* (Nicastro et al. 2016b).
*O V line observed by Liao et al. (2013), is the O II Kβ line [at 556.48(50) eV], confirmed recently by Nicastro et al. (2016a).

Table 7. Comparison of the calibrated energies from the EELS and PES experimental methods (Bizau et al. 2015). The energy difference between the two experimental methods is at most 0.22 eV.

O_2 K shell	EELS	PES	ΔE (eV)
$1s \rightarrow \pi^*$	530.80(20)[a]	530.70(15)	−0.10
$1s \rightarrow 3\sigma$	538.95(4)[b]	539.17(15)	+0.22

Notes. [a]Hitchcock & Brion (1980).
[b]Tanaka et al. (2008).

6 CONCLUSIONS

For the first time, high-resolution photoionization cross-section measurements have been made on Be-like and Li-like atomic oxygen ions in the vicinity of their strong $1s \rightarrow 2p$ resonances and in the $1s \rightarrow np$ resonant region for O^{4+} ions. The measurements are compared with theoretical results from the R-matrix approach, the SCUNC method, and with available satellite observations. Resonance features present in the spectra and predicted by the RMPS method show an excellent agreement with the measurements made at the SOLEIL radiation facility. A detailed comparison of our results (for both systems) is in agreement with predictions from other similar highly sophisticated theoretical approaches. Within the R-matrix approach, we note that both basis sets and models gave suitable results compared to experiment. The collision models with basis set B gave the more favourable results compared to experiment.

A detailed analysis of the resonance parameters indicates some differences with the present SOLEIL experimental results, particularly for the weaker resonance strengths in the O^{4+} spectrum. We speculate that this may be due to the lack of electron correlation included in our theoretical model. We have highlighted various discrepancies with previous satellite observations. Overall the theoretical resonance positions are in suitable agreement with current ground-based SOLEIL experimental measurements. The theoretical cross-section data have been benchmarked against high-resolution measurements and as such would be suitable to be incorporated into data bases such as CLOUDY (Ferland et al. 1998; Ferland 2003), XSTAR (Kallman & Bautista 2001) and ATOMDB (Foster et al. 2012), which are widely used for astrophysical modelling.

ACKNOWLEDGEMENTS

The authors would like to thank the SOLEIL staff, in particular, J. Bozek and S. Nandi, for their helpful assistance during the measurements. We thank F. Nicastro for the provision of the *Chandra* spectra for the blazar Mrk 421 and illuminating discussions on the differences with the *Chandra* observations. T. R. Kallman, at Nasa Goddard, J. C. Raymond and R. K. Smith at the Harvard–Smithsonian Center for Astrophysics are also thanked for discussions on the astrophysical applications. BMMcL acknowledges support from the U.S. National Science Foundation through a grant to ITAMP at the Harvard–Smithsonian Center for Astrophysics, the RTRA network Triangle de la Physique and Queen's University Belfast for the award of a Visiting Research Fellowship (VRF). MFG acknowledges Qatar University for funding support through the startup grant No. QUSG-CAS-DMSP-14/15-4. The R-matrix computational work was performed at the National Energy Research Scientific Computing Center (NERSC), Berkeley, CA, USA, and at the High Performance Computing Center Stuttgart (HLRS) of the University of Stuttgart, Stuttgart, Germany. Grants of computational time at the NERSC and at the HLRS are gratefully acknowledged.

REFERENCES

Al Shorman M. M. et al., 2013, J. Phys. B: At. Mol. Opt. Phys., 46, 195701
Badnell N. R., 1986, J. Phys. B: At. Mol. Opt. Phys., 19, 382
Badnell N. R., 2011, Comput. Phys. Commun., 182, 1528
Ballance C. P., Griffin D. C., 2006, J. Phys. B: At. Mol. Opt. Phys., 39, 3617
Behar E., Rasmuseeen A. P., Blustin A. J., Sako M., Kahn S. M., Kaastra J. S., Branduardi-Raymont G., Steenbrugge K. C., 2003, ApJ, 598, 232
Berkowitz J., 1979, Photoabsorption, Photoionization and Photoelectron Spectroscopy. Academic Press, New York
Berrington K., Quigley L., Zhang H. L., 1997, J. Phys. B: At. Mol. Phys., 30, 5409
Bingcong G., Wensheng D., 2000, Phys. Rev. A, 62, 032705
Bizau J. M. et al., 2016, J. Electron Spectrosc. Relat. Phenom., 210, 5
Bizau J.-M., Cubaynes D., Guilbaud S., Al Shorman M. M., Gharaibeh M. F., Ababneh I. Q., Blancard C., McLaughlin B. M., 2015, Phys. Rev. A., 92, 023401

Downloaded from https://academic.oup.com/mnras/article/465/4/4690/2556152 by Qatar University user on 27 August 2024

Blustin A. J., Branduardi-Raymont G., Behar E., Kaastra J. S., Kahn S. M., Page M. J., Sako M., Steenbrugge K. C., 2002, A&A, 392, 453
Blustin A. J. et al., 2003, A&A, 403, 481
Bruch R., Schmeider D., Schwarz W. H. E., Meinhart M., Johnson B. M., Taulberg K., 1979, Phys. Rev. A, 19, 587
Bruch R., Stolerfohr N., Datz S., Miller P. D., Pepmiller P. L., Yamazaki Y., Krause H. F., Swenson J. K., 1987, Phys. Rev. A, 35, 4114
Burke P. G., 2011, R-Matrix Theory of Atomic Collisions: Application to Atomic, Molecular and Optical Processes. Springer, New York
Cabot S. H. C., Wang Q. D., Yao Y., 2013, MNRAS, 431, 511
Cassinelli J. P., Waldron W. L., Sanders W. T., Harnden Jr F. R., Rosner R., Vaiana G. S., 1981, AJ, 250, 677
Chen M. H., 1985, Phys. Rev. A, 35, 4579
Chen M. H., 1986, At. Data Nucl. Data Tables, 34, 301
Chen M. H., Crasemann B., 1987a, Phys. Rev. A, 35, 4579
Chen M. H., Crasemann B., 1987b, At. Data Nucl. Data Tables, 37, 419
Chen F., Zhang M., Gou B., 2006, J. Phys. B: At. Mol. Opt. Phys., 39, 4249
Davis B. F., Chung K., 1985, Phys. Rev. A, 31, 3017
Davis B. F., Chung K. T., 1989, Phys. Rev. A, 39, 3942
Fano U., Cooper J. W., 1968, Rev. Mod. Phys., 40, 441
Ferland G. J., 2003, ARA&A, 41, 517
Ferland G. J., Korista K. T., Verner D. A., Ferguson J. W., Kingdon J. B., Verner E. M., 1998, PASP, 110, 761
Foster A. R., Ji L., Smith R. K., Brickhouse N. S., 2012, ApJ, 756, 128
Gabriel A. H., 1972, MNRAS, 160, 99
Garcia J., Mendoza C., Bautista M. A., Gorczyca T. W., Kallman T. R., Palmeri P., 2005, ApJ, 779, 78
Gatuzz E. et al., 2013a, ApJ, 768, 60
Gatuzz E. et al., 2013b, ApJ, 778, 83
Gatuzz E., Garcia J., Mendoza C., Kallman T. R., Bautius M. A., Gorczyca T. W., 2014, ApJ, 790, 131
Gorczyca T. W. et al., 2013, ApJ, 779, 78
Gu M. F., Scmidt M., Biersdorfer P., Chen H., Thorn D. B., Träbert E., Behar E., Kahn S. M., 2005, ApJ, 627, 1066
Gupta A., Mathur S., Krongold Y., Nicastro F., Galeazzi M., 2012, ApJ, 597, L8
Gupta A., Mathur S., Galeazzi M., Krongold Y., 2014, Astrophys. Space Sci., 352, 775
Hibbert A., 1975, Comput. Phys. Commun., 9, 141
Hitchcock A. P., Brion C. E., 1980, J. Electron. Spectrosc. Relat. Phenom., 18, 1
Hoffmann G., Müller A., Tinschert K., Salzborn E., 1990, Z. Phys. D – Atoms, Molecules Clusters, 16, 113
Hoffmann G., Müller A., Weiessbeeker K., Stenke M., Tinschert K., Salzborn E., 1991, Z. Phys. D – Atoms, Molecules Clusters, 21, S189
Juett A. M., Schulz N. S., Chakrabarty D., 2004, ApJ, 612, 308
Kaastra J. S., Steenbrugge K., Raasen A. J. J., van der Meer R. L. J., Brinkman A. C., Liedahl D. A., Behar E., de Rosa A., 2002, A&A, 386, 427
Kaastra J. S. et al., 2004, A&A, 428, 57
Kallman T. R., Bautista M. A., 2001, ApJS, 134, 139
Kjeldsen H., Kristensen B., Brooks R. L., Folkman H., Knudsen H., Andersen T., 2002, ApJS, 138, 219
Krongold Y., Nicastro F., Brickhouse N. S., Elvis M., Liedahl D. A., Mathur S., 2003, ApJ, 597, 832
Lee J. C., Ogle P. M., Canizares C. R., Marshall H., Schulz N. S., Morales R., Fabian A. C., Iwasawa K., 2001, ApJ, 554, L13
Liao J. Y., Zhang S.-N., Yao Y., 2013, ApJ, 774, 116
Lin H., Hsue C.-S., Chung K. T., 2001, Phys. Rev A, 65, 032706
McLaughlin B. M., Ballance C. P., 2015, in Resch M. M., Kovalenko Y., Fotch E., Bez W., Kobaysah H., eds, Sustained Simulated Performance 2014. Springer, Berlin, p. 173
McLaughlin B. M., Ballance C. P., Bowen K. P., Gardenghi D. J., Stolte W. C., 2013a, ApJ, 771, L8
McLaughlin B. M., Ballance C. P., Bowen K. P. Gardenghi D. J., Stolte W. C., 2013b, ApJ, 779, L31
McLaughlin B. M., Bizau J.-M., Cubaynes D., Al Shorman M. M., Guilbaud S., Sakho I., Blancard C., Gharaibeh M. F., 2014, J. Phys. B: At. Mol. Opt. Phys., 47, 065201
McLaughlin B. M., Ballance C. P., Pindzola M. S., Müller A., 2015, in Nagel W. E., Kröner D. H., Resch M. M., eds, High Performance Computing in Science and Engineering'14. Springer, Berlin, p. 23
McLaughlin B. M., Ballance C. P., Pindzola M. S., Schippers S., Müller A., 2016, in Nagel W. E., Kröner D. H., Resch M. M., eds, High Performance Computing in Science and Engineering'15. Springer, Berlin, pp 51
McLaughlin B. M., Ballance C. P., Pindzola M. S., Stancil P. C., Schippers S., Müller A., 2017, in Nagel W. E., Kröner D. H., Resch M. M., eds, High Performance Computing in Science and Engineering'16. Springer, Berlin
Mendoza C. et al., 2012, Conference Mapping Oxygen in the Universe, The Reliability of Atomic Data Used for Oxygen Abundance Determinations. Instituto de Astrofisica de Canarias, May 14–18. Available at: http://www.iac.es/congreso/oxygenmap/media/presentations/
Miller M. J., Bergman J. N., 2015, ApJ, 800, 14
Mitnik D. M., Pindzola M. S., Griffin D. C., Badnell N. R., 1999, J. Phys B: At. Mol. Opt. Phys., 32, L479
Moore C. E., 1993, in Gallagher J. W., ed., CRC Series in Evaluated Data in Atomic Physics. CRC Press, Boca Raton, FL, p. 399
Müller A., 2015, Phys. Scr., 5, 054004
Müller A. et al., 2009, J. Phys. B: At. Mol. Opt. Phys., 42, 235602
Müller A. et al., 2010, J. Phys. B: At. Mol. Opt. Phys., 43, 135602
Müller A. et al., 2014, J. Phys. B: At. Mol. Opt. Phys., 47, 135201
Murakami I., Safronova U. I., Kato T., 2002, Can. J. Phys., 80, 1525
Nahar S. N., Pradhan A. K., Zhang H. L., 2001, Phys. Rev. A, 63, 060701
Nicastro F., Senatore F., Gupta A., Guainazzi M., Mathur S., Krongold Y., Elvis M., Piro L., 2016a, MNRAS, 457, 676
Nicastro F., Senatore F., Gupta A., Guainazzi M., Mathur S., Krongold Y., Elvis M., Piro L., 2016b, MNRAS, 458, L123
Nicastro F., Senatore F., Krongold Y., Elvis M., 2016c, ApJ, 828, L12
Nicolosi P., Tondello G., 1997, J. Opt. Soc. Am., 67, 1033
Ogle P. M., Mason K. O., Page M. J., Salvi N. J., Cordova F. A., McHardy I. M., Priedhorsky W. C., 2004, ApJ, 606, 151
Petrini D., Tully J. A., 1991, A&A, 241, 327
Piangos N. A., Nicolaides A., 1993, Phys. Rev. A, 48, 4142
Pinto C., Kaastra J. S., Costantini E., de Vries C., 2013, A&A, 551, 25
Pinto C., Costantini E., Fabian A. C., Kaastra J. S., in'tZand J. J. M., 2014, A&A, 563, A115
Pradhan A. K., 2000, ApJ, 545, L165
Pradhan A. K., Chen G. X., Delahaye F., Nahar S. N., Oelgoetz J., 2003, MNRAS, 341, 1268
Ramírez J., 2013, A&A, 551, A95
Robicheaux F., Gorczyca T. W., Griffin D. C., Pindzola M. S., Badnell N. R., 1995, Phys. Rev. A, 52, 1319
Sakho I., 2011, Rad. Phys. Chem., 80, 1295
Sakho I., 2012, Phys. Rev. A, 86, 052511
Sakho I., Diop B., Faye M., Sène A., Gueye M., Ndao A. S., Biaye M. Wagué A., 2013, At. Data. Nucl. Data Tables, 99, 447
Samson J. A. R., 1967, Techniques of Vacuum Ultraviolet Spectroscopy. Wiley, New York
Schmidt M., Biersdorfer P., Chen H., Thorn D. B., Träbert E., Behar E., 2004, ApJ, 627, 1066
Scully S. W. J. et al., 2005, J. Phys. B: At. Mol. Opt. Phys., 38, 1967
Shore B. W., 1967, Rev. Mod. Phys., 39, 439
Tanaka T. et al., 2008, Phys. Rev. A, 78, 022516
West J., 2001, J. Phys. B: At. Mol. Opt. Phys., 34, R45
Wu L.-J., Xi J.-H., 1991, J. Phys. B: At. Mol. Phys., 24, 3351
Yao Y., Shultz N. S., Gu M. F., Nowak M. A., Canizares C. R., 2009, ApJ, 696, 1418
Zhang S. B., Yeager D. L., 2012a, J. Mol. Struct., 1023, 96
Zhang S. B., Yeager D. L., 2012b, Phys. Rev. A, 85, 032515

This paper has been typeset from a TEX/LATEX file prepared by the author.

Downloaded from https://academic.oup.com/mnras/article/465/4/4690/2556152 by Qatar University user on 27 August 2024